JOURNAL OF MATERIALS SCIENCE 22 (1987) 2739–2750

Microdeformation in partially compatible blends of poly(styrene–acrylonitrile) and polycarbonate

LARRY L. BERGER, EDWARD J. KRAMER
Department of Materials Science and Engineering and the Materials Science Center, Cornell University, Ithaca, New York 14853, USA

Dilute 3-component 1-phase solutions in methylene chloride of poly(styrene–acrylonitrile) PSAN and polycarbonate PC are used to cast phase separated thin films. Films of pure PSAN, pure PC and five intermediate compositions are examined. The films are bonded to copper grids and strained at a constant rate of $4.1 \times 10^{-6}\,\text{sec}^{-1}$. The median tensile strain ε_v for void formation is determined using an optical microscope and the regions surrounding the voids are examined by TEM. At room temperature and slow strain rates both PSAN and PC plastically deform by shear yielding. For pure PSAN ε_v was found to be ~ 0.13 whereas for PC ε_v exceeds 0.23. The addition of the more ductile polymer PC to PSAN at weight fractions x for $x \leqslant 0.4$ decreases ε_v. In this case voids form in crazes at the boundaries between the PC-rich inclusion and the PSAN-rich matrix. When the PC content is increased to $x = 0.8$, ε_v approaches 0.23. The effect of physical ageing (annealing below T_g the glass transition temperature) on the mode of plastic deformation was also examined over the same compositional range. Physical ageing was found to suppress shear deformation and favour crazing in PSAN and PSAN-rich phases. Because crazes are more susceptible to breakdown than DZ's (shear deformation zones), physical ageing results in a marked decrease in ε_v. The breakdown statistics of these phase separated partially compatible blends was found to follow a Weibull distribution in strain from which two parameters may be extracted: ϱ the Weibull modulus and ε_w the Weibull scale parameter. ϱ is a measure of the breadth of distribution of void initiation and ε_w is a measure of the median strain to void formation in the films. The behaviour of ε_w was found to approximately mirror ε_v. The Weibull modulus ϱ appears to be primarily controlled by the matrix phase.

1. Introduction

Due to the low entropy of mixing for long chain polymers most polymer pairs are at best only partially compatible and will phase separate [1–9]. For the case where the T_g, the glass transition temperature, of each of the components is well above room temperature a phase separated glassy material results. These phase separated blends have the potential to offer many unique and useful mechanical properties unattainable in either a pure homopolymer or copolymer. However before these materials may be reliably used an understanding of the plastic deformation mechanisms in the blend is essential. Unfortunately most studies of mechanical properties in glassy blends have focused on the bulk macroscopic deformation and not on the more fundamental microscopic plastic deformation in each of the phases (which is usually on a scale of the order of 0.1 to 100 μm).

In this paper we use both optical microscopy and TEM to study the plastic deformation behaviour in thin films of glassy blends of two commercially important polymers, polycarbonate and poly(styrene–acrylonitrile). These polymers are only partially compatible. In addition we make use of a simple test [10, 11] to quantitatively determine the statistics of void and crack formation in the thin films. Lastly we examine the effects of physical ageing (annealing below T_g) on the plasticity in these films and its effect on the void formation statistics.

2. Experimental details

Dilute 3-component 1-phase solutions of poly(styrene–acrylonitrile) (PSAN) (Dow Chemical Co., Midland, Michigan, USA) and polycarbonate (PC) in methylene chloride were prepared with the following $\text{PSAN}_{1-x}/\text{PC}_x$ weight ratio where $x = 0.0$, 0.2, 0.4, 0.5, 0.6, 0.8 and 1.0. The PSAN used was a random copolymer having a weight average molecular weight $\bar{M}_w = 160\,\text{K}$ and an acrylonitrile content of 25%. The PC resin was a GE Lexan having an intrinsic viscosity $[\eta] = 0.661\,\text{dl g}^{-1}$ and a weight average molecular weight $\bar{M}_w = 39\,\text{K}$. Methylene chloride is a good solvent for both the PC and the PSAN.

Prior to casting the glass slides were cleaned with acetone to remove grease and pressurized N_2 gas was used to blow away dust from the surface of the slides.

0022–2461/87 $03.00 + .12

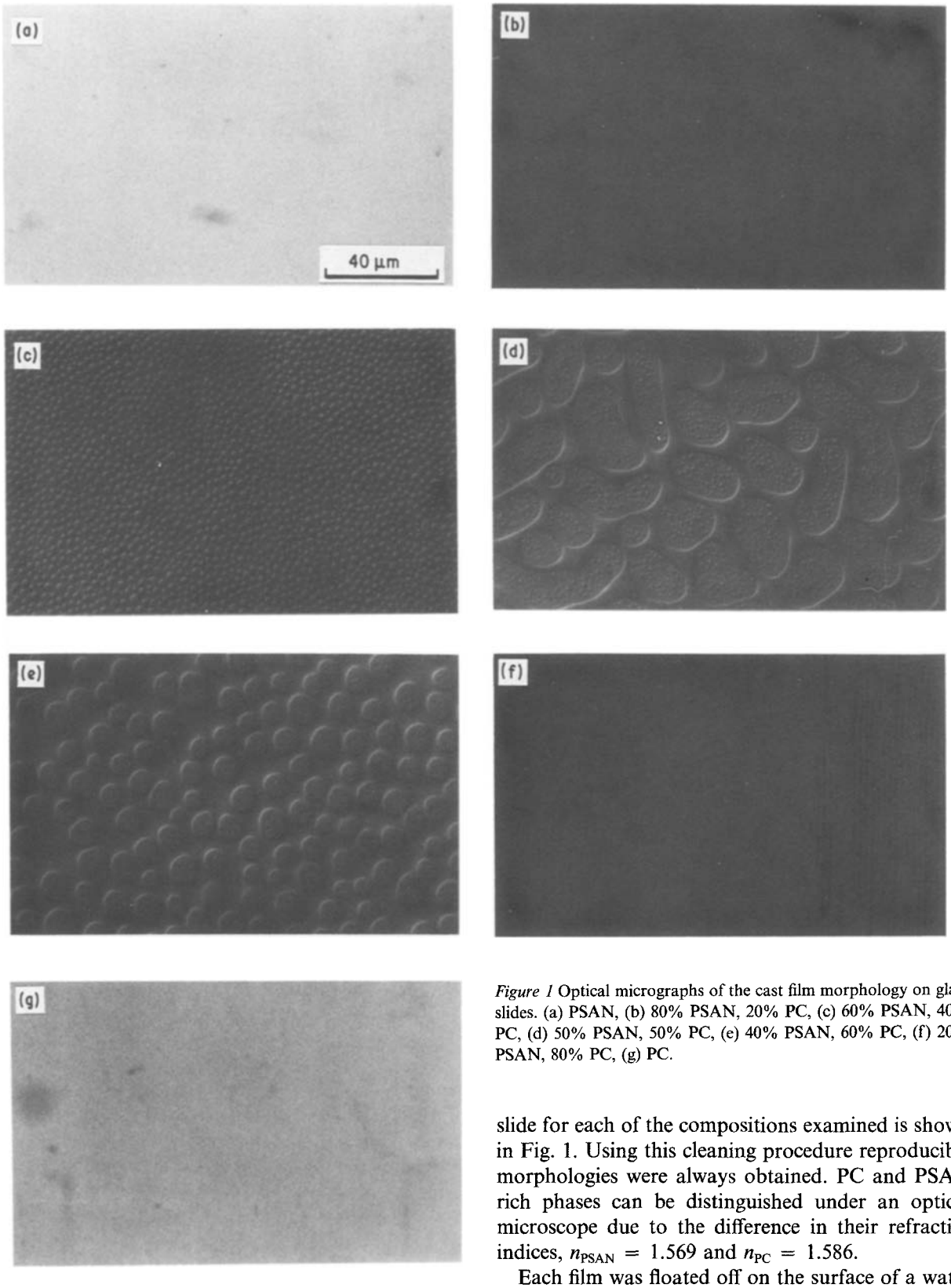

Figure 1 Optical micrographs of the cast film morphology on glass slides. (a) PSAN, (b) 80% PSAN, 20% PC, (c) 60% PSAN, 40% PC, (d) 50% PSAN, 50% PC, (e) 40% PSAN, 60% PC, (f) 20% PSAN, 80% PC, (g) PC.

To further reduce the dust concentration the polymer–solvent solutions were filtered through a porous ceramic filter to remove any particles greater than 20 μm in size. Uniform films were produced by drawing glass slides from the solution at a constant rate. In all cases the film thickness, measured by a Zeiss interference microscope, was held constant at 0.4 μm. This control is achieved by adjusting the total polymer to solvent concentration while maintaining the desired ratio between the two polymers. After solvent evaporation the resulting phase morphology on the glass slide for each of the compositions examined is shown in Fig. 1. Using this cleaning procedure reproducible morphologies were always obtained. PC and PSAN rich phases can be distinguished under an optical microscope due to the difference in their refractive indices, $n_{PSAN} = 1.569$ and $n_{PC} = 1.586$.

Each film was floated off on the surface of a water bath and picked up on a well annealed copper grid previously coated with the same polymer [12]. A short exposure to the methylene chloride vapour served to remove any slack in the film and ensure bonding between the film and the grid. The grid subdivides the film into ~ 40 independent grid squares each having an area of 1 mm^2.

One day after preparation the grids were mounted in a strain frame coupled to a motor drive and strained in tension at a strain rate of 4.1×10^{-6} sec^{-1}. Any grid squares that were poorly bonded or had traces of dust were eliminated from consideration. As the film

TABLE I Types of phase separation resulting from casting from dilute solution at room temperature

PSAN (wt %)	Phase separation	Multiple phase separation	Continuous phase	Average diameter of minority phase
100	No	No	PSAN	–
80	Yes	No	PSAN-rich	0.4–0.7 μm
60	Yes	No	PSAN-rich	1.4–1.9 μm
50	Yes	Yes	PC-rich	PSAN (islands) 10–20 μm PC-rich (incl.) 0.4–0.6 μm PSAN (incl.) 0.25–0.35 μm
40	Yes	Yes	PC-rich	PSAN (islands) 5–8 μm PC-rich (incl.) 0.4–0.6 μm PSAN (incl.) 0.25–0.35 μm
20	Yes	No	PC-rich	0.2–0.4 μm
0	No	No	PC	–

was strained, the initiation of void formation was observed in each grid square using an optical microscope at 50 × magnification. Observations were made at roughly 1 h intervals to determine the number fraction of grid squares exhibiting void formation p_v [10]. Although the phase morphology differs markedly for the various compositions a consistent criterion was used to determine the onset of void formation. Void formation (detected as a dark spot in reflected light) was chosen to be any equiaxed hole of at least 50 μm in diameter. In this manner a quantitative breakdown strain ε_v, defined as the median strain to produce at least one void in one half of the grid squares, could be determined.

The effect of physical ageing on the plastic deformation mechanisms and breakdown statistics was also studied. Samples were prepared in the manner previously described for fresh (unaged) films but prior to straining were subjected to an anneal at 85 to 90° C for 1 h and allowed to cool to room temperature. Since the ageing temperature is below the T_g of the lower T_g component no change in phase morphology occurs due to ageing. The same criterion used to determine ε_v for unaged samples was used to determine ε_v for this class of samples. Since the low magnification employed in determining ε_v does not allow for the earliest possible determination of void formation all the compositions examined (both aged and unaged) were observed in the TEM. In this case the samples were strained up to $p_v \approx 0.4$, a selected grid square was cut out and the void initiation site was examined more closely by TEM.

3. Results

3.1. Morphology

For all the intermediate compositions examined here it was found that PSAN and PC blends phase separate. Table I shows the type of phase separation resulting from casting from dilute solution at room temperature. The addition of PC to PSAN to form $PSAN_{1-x}PC_x$ blends results in a simple phase separation up to $x = 0.4$ with a PSAN-rich continuous phase containing roughly equiaxed inclusions of PC-rich phase. Further additions of PC result in a more complex morphology. For the blends of $PSAN_{0.5}PC_{0.5}$ and $PSAN_{0.4}PC_{0.6}$, a PC-rich continuous phase containing both PSAN-rich "islands" and PSAN-rich inclusions form. The PSAN-rich "islands" however contain even smaller PC-rich inclusions within them. This phase inversion probably occurs because the initial PSAN-rich phase which separates as the solvent evaporates contains too much PC which subsequently precipitates within the PSAN as more solvent is removed. When x is increased to $x = 0.8$ a simple morphology again results, with a PC-rich continuous phase containing roughly equiaxed PSAN-rich inclusions.

3.2. Microdeformation of unaged samples

At a slow strain rate of $4.1 \times 10^{-6}\,sec^{-1}$ fresh (unaged) films of pure PSAN deform by shear deformation with little or no crazing present. When the strain rate is increased the propensity for both strain localization and crazing increases. At a strain rate $4.1 \times 10^{-4}\,sec^{-1}$ competition between crazing and shear deformation results. Crazes are typically found to nucleate from dust particles where the stress is highest and then as the stress in the film drops shear deformation is favoured. This behaviour has been noted previously for PSAN [13]. As the strain rate is increased to $4.1 \times 10^{-2}\,sec^{-1}$ only narrow deformation zones form in addition to crazes, but many of the craze tips are blunted by shear deformation. The typical forms of local deformation found at these three strain rates are shown in Fig. 2.

By contrast the deformation in pure PC films was found to be insensitive to strain rate over the same range. Even at the highest strain rates of $10^{-2}\,sec^{-1}$ only diffuse shear deformation zones [14] were found with no crazes present.

For the quantitative tests to determine the breakdown strain ε_v for void formation the slowest strain rate of $4.1 \times 10^{-6}\,sec^{-1}$ was used. Optical micrographs of a single grid square of unaged PSAN, PC and the five intermediate blend compositions at $p_v \approx 0.5$ are shown in Fig. 3. Although the phase

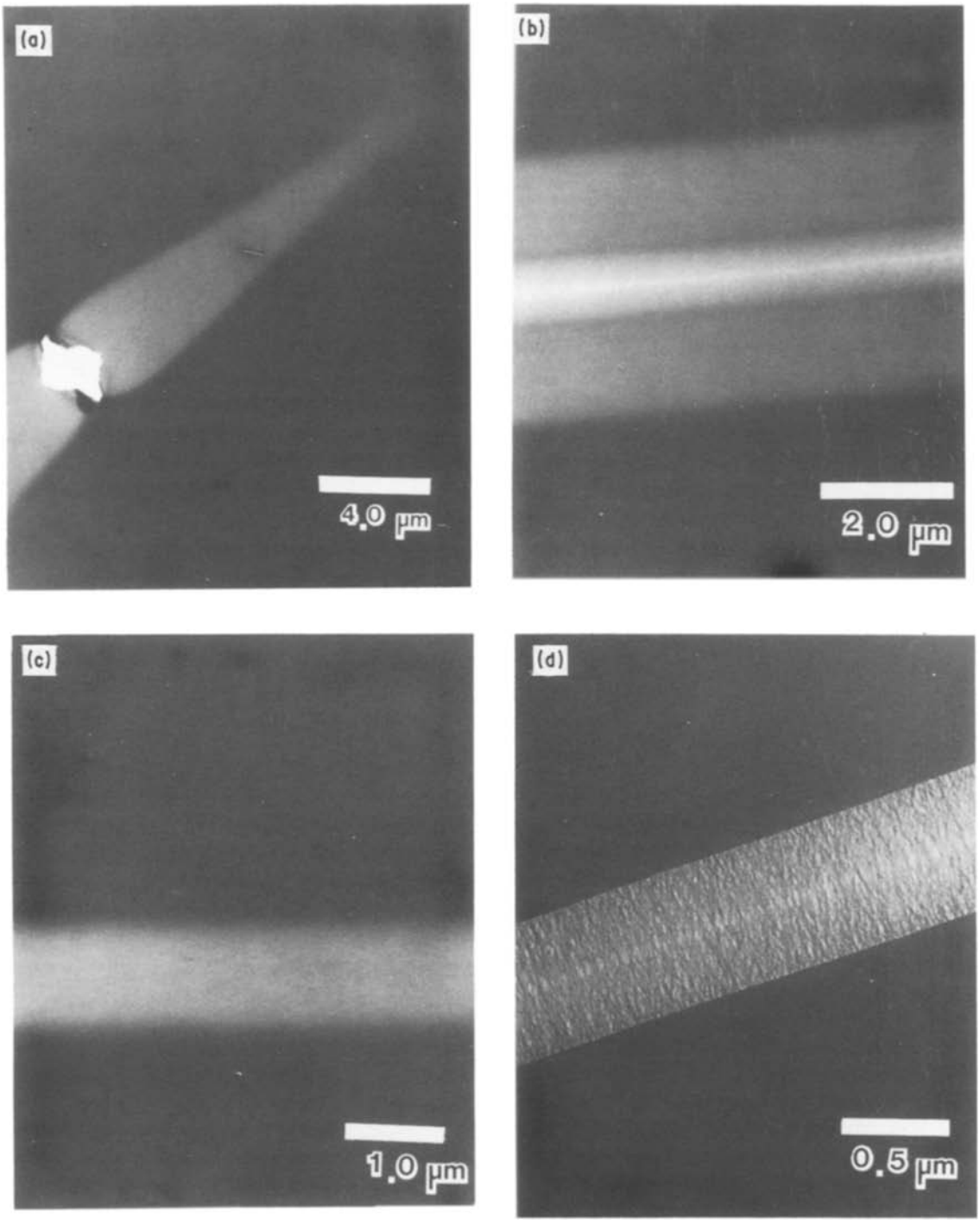

Figure 2 TEM micrographs of plastic deformation in PSAN as a function of strain rate. (a) $\dot{\varepsilon} = 4.1 \times 10^{-6}\,\text{sec}^{-1}$, (b) $\dot{\varepsilon} = 4.1 \times 10^{-4}\,\text{sec}^{-1}$, (c) $\dot{\varepsilon} = 4.1 \times 10^{-4}\,\text{sec}^{-1}$, (d) $\dot{\varepsilon} = 4.1 \times 10^{-2}\,\text{sec}^{-1}$.

morphology can not be seen at this low magnification, large differences in the resulting plastic deformation are apparent between one blend and the next. Comparing the neat PSAN and PC it can be seen that at a strain of 0.16 the PC exhibits only diffuse deformation whereas the PSAN has considerable void formation within DZ's. Fig. 4 shows how ε_v changes as a function of weight fraction PC for unaged films (open diamonds). For pure PSAN ε_v was found to be approximately 0.13 whereas for pure PC ε_v exceeds 0.23, the strain at which the copper grid usually fails. At this strain the percentage of grid squares having at least one void was usually less than 20%. Extrapolation of ε_v for pure PC using the Weibull analysis to be discussed later yields a value greater than 0.50.

The addition of the more ductile PC to PSAN initially decreases its ε_v. Although crazes were not present in the fresh films of PSAN the addition of PC causes crazing in the PSAN-rich phase and subsequent void formation via craze breakdown at the boundary between the two phases. TEM micrographs of selected regions in a given grid square for two pure polymers and each of the blends are shown in Fig. 5. Profuse crazing can be seen in the $PSAN_{0.8}PC_{0.2}$ blend (Fig. 5b) and to a lesser extent in the other intermediate compositions. The arrows in Fig. 6 point to small voids

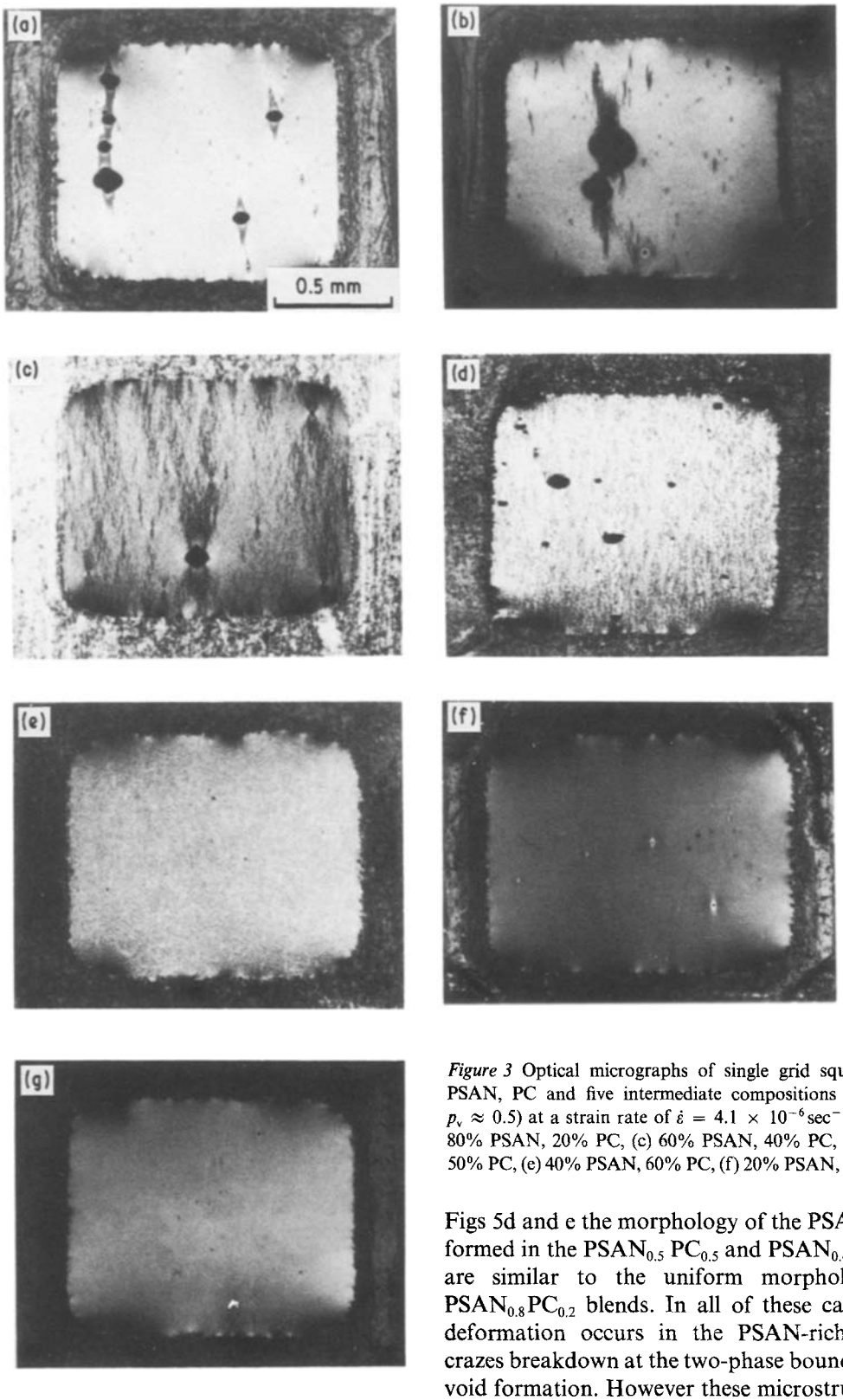

Figure 3 Optical micrographs of single grid squares of unaged PSAN, PC and five intermediate compositions strained (up to $p_v \approx 0.5$) at a strain rate of $\dot{\varepsilon} = 4.1 \times 10^{-6}\,\text{sec}^{-1}$. (a) PSAN, (b) 80% PSAN, 20% PC, (c) 60% PSAN, 40% PC, (d) 50% PSAN, 50% PC, (e) 40% PSAN, 60% PC, (f) 20% PSAN, 80% PC, (g) PC.

resulting from craze breakdown at the interface between the PSAN-rich phase (light) and the PC-rich inclusion (dark)* for an $x = 0.2$ blend. Note that in all cases these voids do not result from direct deadhesion of the PSAN/PC interfaces; rather a craze which grows in the PSAN-rich phase adjacent to the PC-rich inclusion undergoes craze breakdown. As shown in Figs 5d and e the morphology of the PSAN "islands" formed in the $PSAN_{0.5}\,PC_{0.5}$ and $PSAN_{0.4}PC_{0.6}$ blends are similar to the uniform morphology of the $PSAN_{0.8}PC_{0.2}$ blends. In all of these cases the local deformation occurs in the PSAN-rich phase and crazes breakdown at the two-phase boundary, causing void formation. However these microstructures differ in that voids formed in the "islands" do not propagate into catastrophic cracks; in this case the growth of a void is arrested at the PC-rich continuous phase boundary. No crack arrest mechanism exists for the PSAN-rich blends and therefore the voids grow relatively rapidly to form cracks of critical size.

In the $PSAN_{0.2}PC_{0.8}$ blends no crazing was observed. Presumably crazes could not nucleate in the small

*In the TEM micrographs of the undeformed films the PC-rich phase will appear darker than the PSAN-rich phase due to the mass thickness contrast caused by the higher oxygen content of the PC phase. This difference in contrast is enhanced in the deformed films because under uniaxial extension the PSAN-rich phase will be "thinned" relative to the PC-rich phase. This relative thinning results from a higher draw ratio λ in the PSAN-rich crazes and DZs than in the PC-rich DZs.

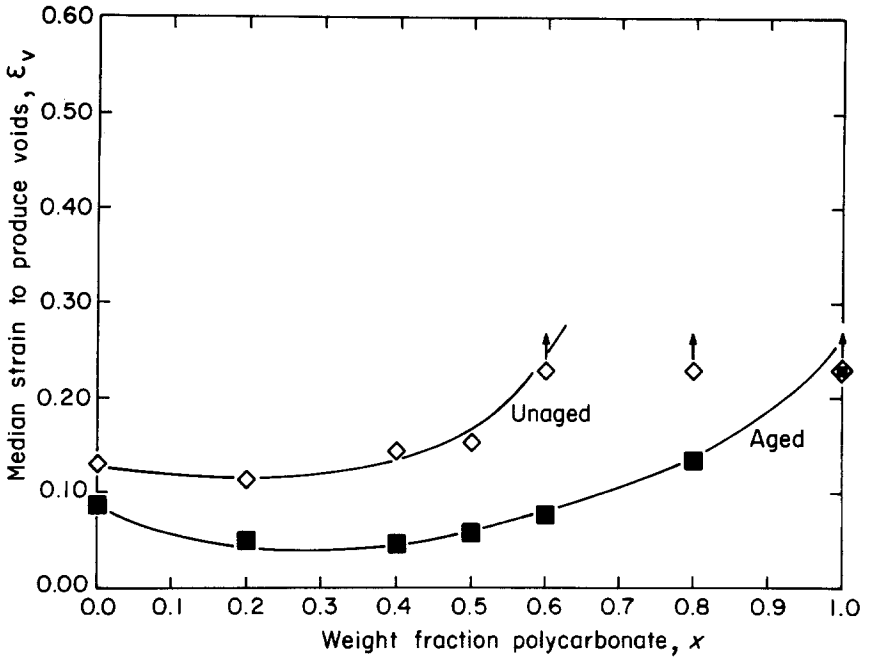

Figure 4 The median strain ε_v plotted as a function of x, weight fraction PC, for films strained at $\dot{\varepsilon} = 4.1 \times 10^{-6}\,\text{sec}^{-1}$. (◇) Unaged, (■) aged.

isolated PSAN-rich spherical domains*. In these samples, like the neat PC, only diffuse shear deformation was found. These samples also had an ε_v that exceeded 0.23. Extrapolation to determine ε_v gives values near 0.50.

3.2. Microdeformation of aged samples

The breakdown strain ε_v was determined for films aged for 1 h at 85 to 90° C, for the same compositions as the unaged films. Shown in Fig. 7 are the optical micrographs of individual grid squares for the aged samples strained (up to $p_v \approx 0.5$) at the same slow strain rate of $4.1 \times 10^{-6}\,\text{sec}^{-1}$. It is apparent that the nature of the plasticity is changed from that of the unaged samples for all the compositions. For pure PSAN the predominant mode of deformation was crazing; shear deformation was almost completely suppressed. The PC exhibited strain localization

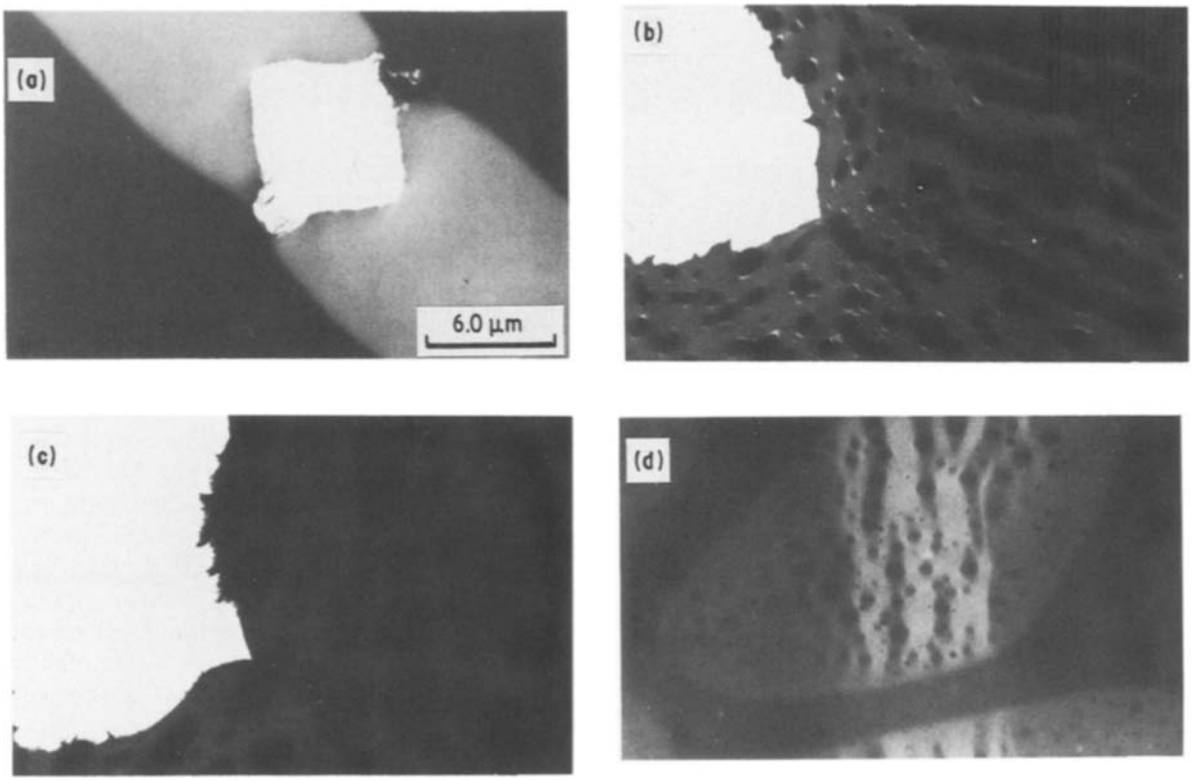

Figure 5 TEM micrographs of selected regions in a given grid square (at $p_v \approx 0.4$) for unaged samples. (a) PSAN, (b) 80% PSAN, 20% PC, (c) 60% PSAN, 40% PC, (d) 50% PSAN, 50% PC, (e) 40% PSAN, 60% PC, (f) 20% PSAN, 80% PC, (g) PC.

*Due to the small size of the PSAN-rich inclusions (~200 nm) the formation of craze fibrils at the craze tip is suppressed. In order for craze fibril spacings (which are typically ~20 to 100 nm) to form the volume of the inclusion must be around an order of magnitude larger than the fibril spacing.

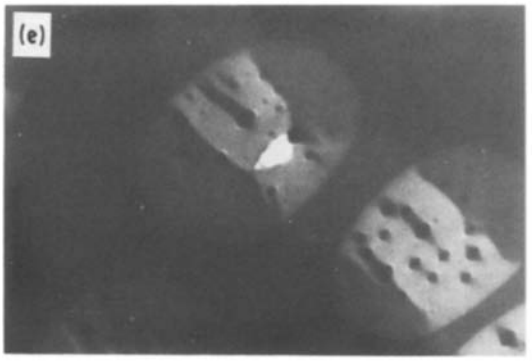

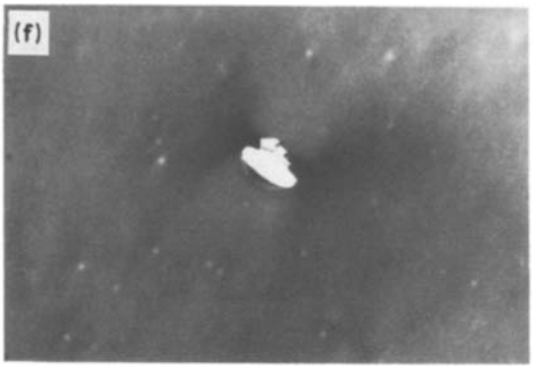

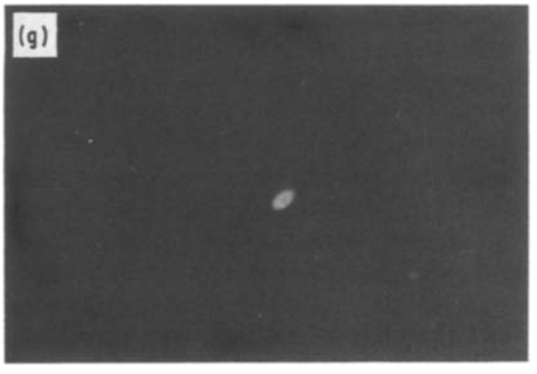

Figure 5 Continued.

resulting in wide plane stress deformation zones with sharp shoulders [14]. The breakdown strain ε_v is plotted as a function of composition for the aged samples (filled squares) in Fig. 4. For all compositions except pure PC physical ageing causes a significant decrease in ε_v. Although a change in the strain localization in the pure PC can be seen (cf. Figs 3g and 7g), no decrease in ε_v was measured. The TEM micrographs of selected regions of individual grid squares are shown in Fig. 8. Crazes were found to nucleate from dust particles and the grid bars for pure PSAN and voids formed at the boundary between the craze and the undeformed bulk polymer. This behaviour is similar to that previously reported [10, 11] for polystyrene crazes, but differs from that reported for polymethylmethacrylate crazes [15], the latter breaking down in the oldest portion of the craze, the centre or midrib.

The addition of PC to PSAN for $x < 0.4$ decreases ε_v. Again even though pure PC is much more ductile than pure PSAN the addition of PC makes the blend more fragile. In the blends with a continuous PSAN-rich phase as the craze advances through this matrix it encounters PC-rich inclusions and attempts to grow around them. The arrows pointing in the direction of the path of such a craze tip are shown in Fig. 9. A non-planar craze tip path results in large strains in the matrix around the inclusion and may induce void formation at the boundary. For the $PSAN_{0.2}PC_{0.8}$ no void formation was observed at the two-phase boundary. Here voids formed at the dust particles which served to first nucleate the deformation zone. In these samples it appears that the voids form when the polymer debonds from the "dust" particles. The breakdown voids in these samples were similar to those voids of pure PC, which appeared as small diamond shape cavities [14, 16–18].

3.3. Breakdown statistics

The breakdown of these polymer films to form voids follows Weibull statistics [10, 19, 20]. Under the assumption that void formation is a Poisson process uniformly distributed over the volume of the film, the probability p of at least one void forming in one grid square may be expressed as a Weibull distribution:

$$p(\varepsilon) = 1 - \exp\left[-(V_0/V_b)(\varepsilon/\varepsilon_w)^{\varrho}\right] \quad (1)$$

where V_0 and V_b are the initial volume of a grid square and a reference volume, respectively (for these grids $V_0/V_b = 1$), ε is the total strain and ϱ and ε_w are the Weibull modulus and scale parameter respectively. Equation 1 may be rewritten as:

$$\ln\{\ln[1/(1-p)]\} = \varrho \ln \varepsilon - \varrho \ln \varepsilon_w + \ln(V_0/V_b) \quad (2)$$

A plot of $\ln\{\ln[1/(1-p)]\}$ against $\ln \varepsilon$ should yield a straight line from which the Weibull scale parameter ε_w and the Weibull modulus ϱ can be determined from the y-intercept and slope, respectively. The Weibull scale parameter ε_w is a measure of the stability of the local plastic deformation in the film. Previously ε_w has been shown to be a measure of craze fibril stability in polystyrene [10, 11]. The Weibull modulus ϱ is a measure of the breadth of the distribution of either craze or deformation zone breakdown. Narrow distributions produce high ϱ and vice versa.

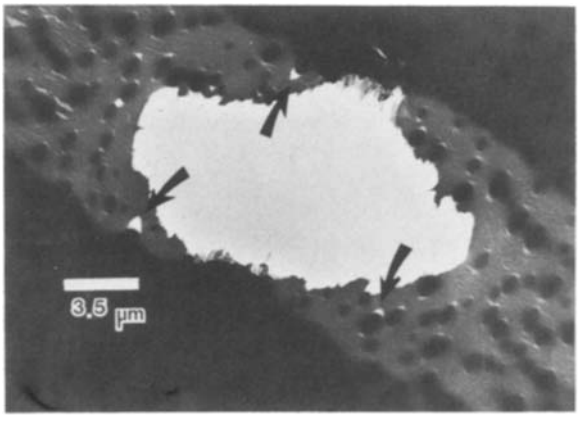

Figure 6 Arrows pointing to small voids formed in crazes at the boundary between the PC-rich phase and the PSAN-rich phase for a $x = 0.2$ blend.

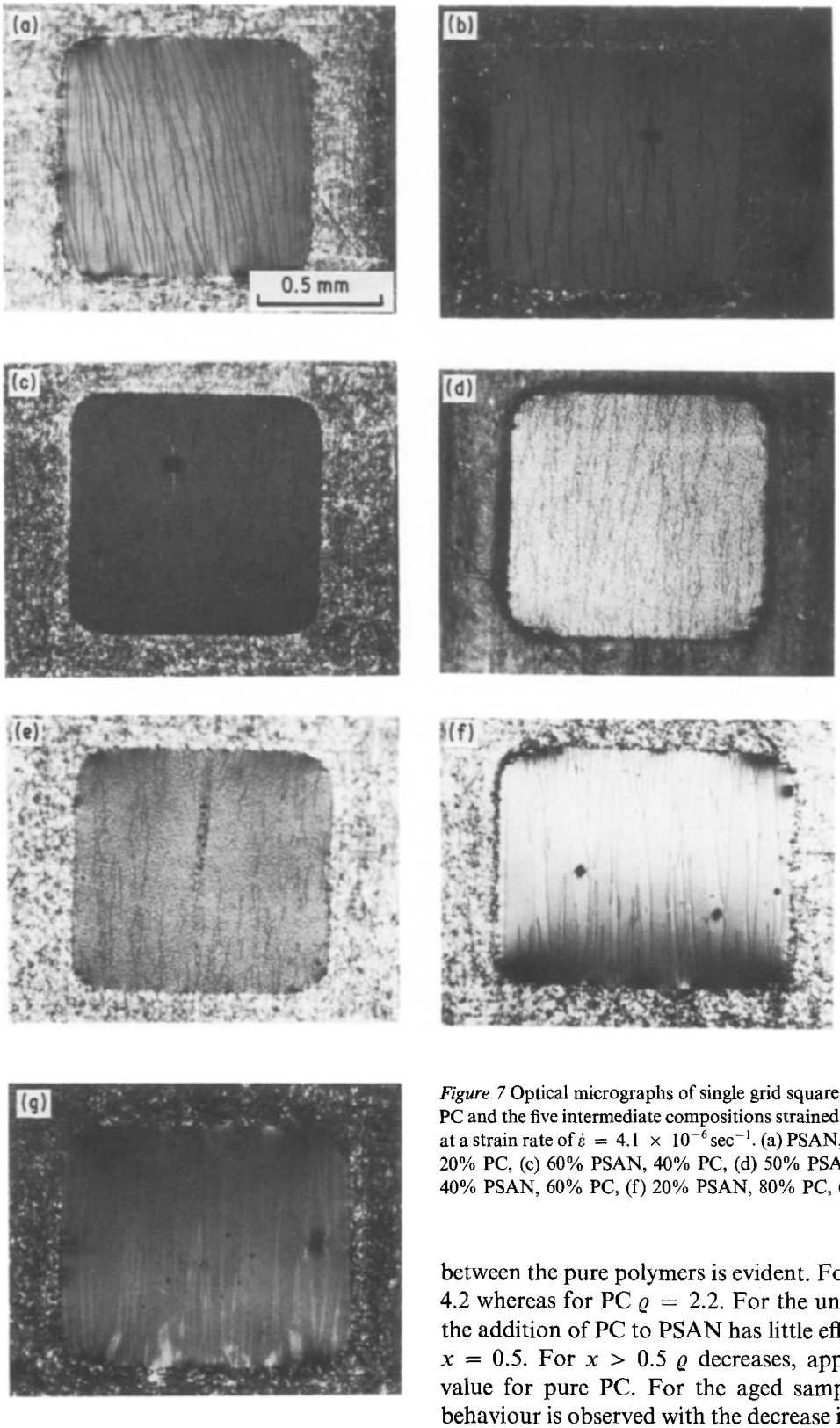

Figure 7 Optical micrographs of single grid squares of aged PSAN, PC and the five intermediate compositions strained (up to $p_v \approx 0.5$) at a strain rate of $\dot{\varepsilon} = 4.1 \times 10^{-6}\,\text{sec}^{-1}$. (a) PSAN, (b) 80% PSAN, 20% PC, (c) 60% PSAN, 40% PC, (d) 50% PSAN, 50% PC, (e) 40% PSAN, 60% PC, (f) 20% PSAN, 80% PC, (g) PC.

Fig. 10 shows typical Weibull plots for aged samples of pure PSAN, pure PC and a blend with $x = 0.5$. Clearly the data follow a Weibull distribution*. Similar plots were made for all the compositions, aged and unaged, to determine ϱ and ε_w. A plot of ϱ against x, the weight fraction of PC in the blend, is shown in Fig. 11. The open and closed circles correspond to the unaged and aged samples, respectively. The difference between the pure polymers is evident. For PSAN $\varrho = 4.2$ whereas for PC $\varrho = 2.2$. For the unaged samples the addition of PC to PSAN has little effect on ϱ until $x = 0.5$. For $x > 0.5$ ϱ decreases, approaching the value for pure PC. For the aged samples a similar behaviour is observed with the decrease in ϱ occurring at $x \approx 0.6$. The change in deformation mechanism from shear deformation to crazing in the PSAN-rich blends upon ageing is reflected in a 50% increase in ϱ. This difference is maintained as long as the continuous phase is PSAN. It disappears for the PC-rich blends where there is no change in deformation mechanism on ageing. The Weibull scale parameter ε_w is plotted as a function of x in Fig. 12. The open and closed circles correspond to the unaged and aged samples, respectively.

*For unaged samples of pure PC and the blend $PSAN_{0.2}PC_{0.8}$ which have immeasurably high ε_v's, the Weibull plots typically had only a few points. This small number of data points will of course reduce the accuracy of both ϱ and ε_w for these two samples.

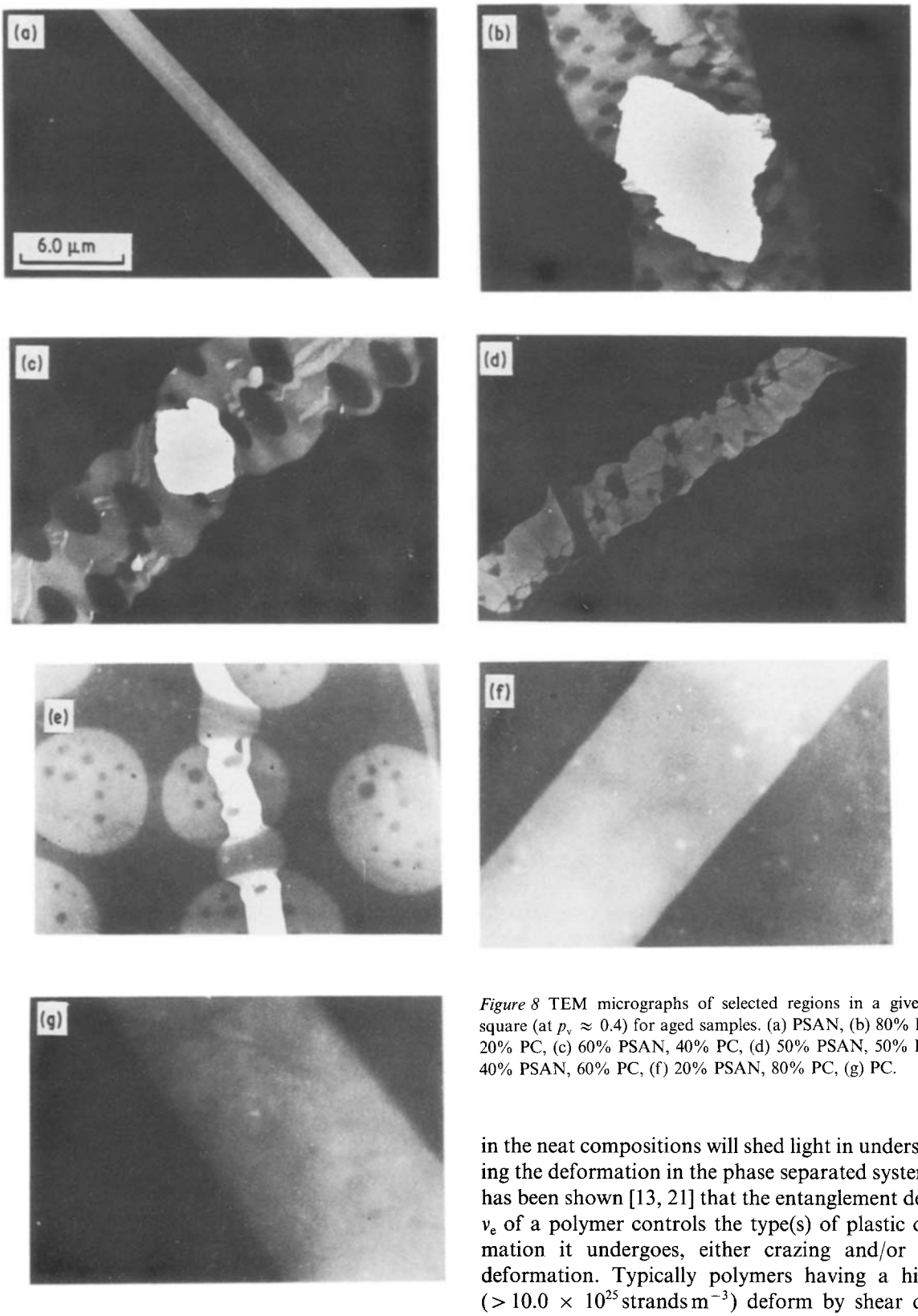

Figure 8 TEM micrographs of selected regions in a given grid square (at $p_v \approx 0.4$) for aged samples. (a) PSAN, (b) 80% PSAN, 20% PC, (c) 60% PSAN, 40% PC, (d) 50% PSAN, 50% PC, (e) 40% PSAN, 60% PC, (f) 20% PSAN, 80% PC, (g) PC.

For unaged samples ε_w decreases slightly with x for $x < 0.5$ and then increases markedly as x is increased further. A similar trend is found for aged samples with the increase in ε_w occurring between $x = 0.6$ and $x = 0.8$. The behaviour of ε_w approximately mirrors that of ε_v.

4. Discussion

The higher ductility of pure PC relative to pure PSAN is reflected in the higher values of ε_v for PC in both the aged and unaged samples. Examining the deformation in the neat compositions will shed light in understanding the deformation in the phase separated systems. It has been shown [13, 21] that the entanglement density v_e of a polymer controls the type(s) of plastic deformation it undergoes, either crazing and/or shear deformation. Typically polymers having a high v_e ($> 10.0 \times 10^{25}$ strands m^{-3}) deform by shear deformation and polymers having a low v_e deform by crazing [22]. For polymers having v_e between these values both types of deformation have been observed in the same film. The v_e in PSAN and PC are 6×10^{25} and 29×10^{25} strands m^{-3}, respectively. The v_e will also control how rapidly the polymer will strain harden while plastically deforming, the high v_e polymers strain hardening more rapidly than the low v_e polymers.

The effects of dissimilar strain hardening rates in phase separated systems will control the stresses at the phase boundary in the deformed state. Consider

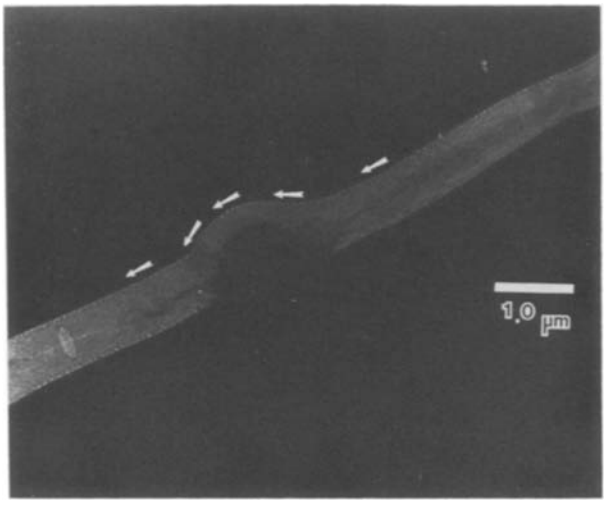

Figure 9 Arrows pointing in the direction of a craze tip in a PSAN-rich matrix that grew around a PC-rich inclusion for a $x = 0.4$ blend.

the unaged samples with $0.2 < x < 0.6$ shown in Figs 5b to e. When the applied stress σ exceeds the yield stress σ_y of the PC-rich inclusion, it will plastically deform and begin to strain harden. The strain hardening within the inclusion will require the applied stress to increase if the plastic flow is to continue. If σ continues to increase and exceeds σ_y of the PSAN-rich matrix, this phase will also plastically deform. Now as both phases plastically deform the PC rich inclusion will strain harden more rapidly than the PSAN-rich matrix that surrounds it. The incompatibility in plastic strain that develops between the PSAN-rich matrix and the PC-rich inclusion leads to high tensile stresses at the poles of the PC-rich inclusion. (We define the poles of the inclusion as the points on its surface where the axis of maximum principal strain is normal to the surface.) This high tensile stress results in craze formation which is favoured in the PSAN-rich matrix at higher stresses and strain rates. This behaviour is different from that found in the rubber modified PSAN, ABS (acrylonitrile-butadiene-styrene). In that case crazes nucleate at the equator of the rubber inclusion [23]. The behaviour observed for the PC–PSAN blends is that expected when there is good adhesion across the boundary and the inclusion is "stiffer" than the matrix [24]. When x was increased to $x = 0.4$ less crazing was observed around the PC rich inclusions. It appears that the larger inclusions can better accommodate the total strain. At $x = 0.5$ and $x = 0.6$ voids formed in deformation zones contained within the PSAN-rich "islands". Here too the deformation zones encompassing the PC-rich inclusions form crazes and the crazes break down to form voids at the two-phase boundary. An early stage of void formation within a PSAN-rich "island" for a $x = 0.6$ blend is shown in Fig. 5e. At $x = 0.8$ only diffuse shear deformation zones were observed producing only a small decrease in ε_w for this blend relative to pure PC.

A different behaviour is found in the aged samples. Physical ageing is known to suppress shear deformation and favour crazing in PSAN [13]. Similar ageing treatments in PC do not cause crazing but do cause strain localization [14] and embrittlement [25–27] in impact tests.

The embrittlement in macroscopic samples of PSAN due to ageing is mirrored by a decrease in ε_v from 0.138 to 0.078 in the thin films. In pure PSAN this decrease reflects the difference in breakdown mechanism occurring during ductile (shear) and brittle (crazing) deformation. Crazing in the continuous PSAN-rich phase has the effect of decreasing ε_v for all compositions. Crazes are more susceptible to breakdown than DZs in the PSAN-rich phase. For the blend $PSAN_{0.2}PC_{0.8}$ ageing results in marked strain localization in the deformation zone. In this case however no crazing was found in either the PSAN-rich inclusion or the PC-rich matrix. Although ε_v for this composition was decreased on ageing, preferential breakdown was not observed in the inclusion or at its boundary with the PC-rich phase.

The voids formed by the breakdown of either a craze or DZ in PSAN are quite different. In the case of crazing fibril breakdown occurs when the craze bulk interface encounters a flaw or "seed" which is severe enough to produce a void. In contrast the

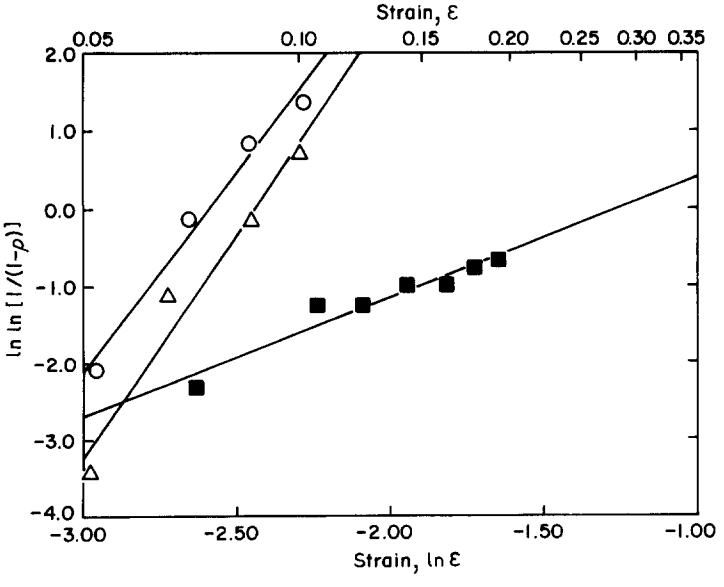

Figure 10 Typical Weibull plots of ln {ln [1/(1 − p)]} against ln ε for void formation at a strain rate of $\dot{\varepsilon} = 4.1 \times 10^{-6}\,sec^{-1}$. (△) aged PSAN, (○) aged $PSAN_{0.5}PC_{0.5}$, (■) aged PC.

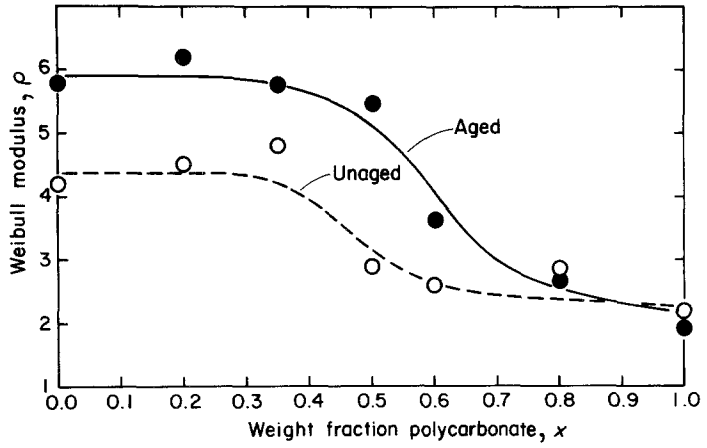

Figure 11 Weibull modulus ϱ as a function of x, weight fraction PC. (○) unaged, (●) aged.

formation of a void in a DZ (in both PC and PSAN) usually occurs at its initiation site by the debonding of the polymer from a "dust" inclusion. Although the precise mechanism for void formation in either a craze or DZ is not well understood, it is reasonable to assume that it depends on the local stress at the flaw.

In what follows we postulate that the drawing stress in either the craze-bulk or DZ-bulk interface increases as a power law of the strain ε, i.e.,

$$\sigma = \sigma_0(\varepsilon)^\gamma \tag{3}$$

where $\sigma_0 > 0$ and $\gamma \geqslant 0$ are constants. We further assume that the breakdown to form a void in either a craze or DZ occurs at natural flaws or "seeds" in the film and that the "seed" density Λ for void formation depends on a power law of the stress, ie.

$$\Lambda(\sigma) = (\sigma/\sigma_b)^\delta/V_b, \qquad \sigma > 0 \tag{4}$$

where V_b, σ_b and δ are positive constants for each blend. (For convenience V_b will be chosen to be the volume of one grid square (0.4×10^{-3} mm^3) in which one breakdown seed will be encountered at a stress σ_b.)

Substituting Equation 4 into Equation 3, Λ may be rewritten as

$$\Lambda(\sigma) = (\sigma_0^\delta \varepsilon^{\gamma\delta})/V_b\sigma_b^\delta \tag{5}$$

Assuming all void formations are statistically independent, ϱ may be related to δ and γ by the following expression [10]:

$$\varrho = \delta\gamma + 1 \tag{6}$$

Now if the seeds are randomly distributed within the initial volume, and the strain rate in the film is constant, the hazard rate of encountering a seed should be constant with the strain as more material is plastically deformed. Assuming that the weak spots are time independent and that the drawing stress is constant with increasing strain, the strain at void formation should follow a Weibull distribution, Equation 1, with Weibull modulus $\varrho = 1$. However values of ϱ greater than one are consistently observed for the film squares. Therefore in these experiments it appears that the drawing stress σ increases with strain ε,* so that the term $(\varepsilon/\varepsilon_w)^\varrho$ in Equation 1 actually reflects the stress dependence of void formation through Equation 3.

The data in Fig. 11 suggests that the deformation mechanism in the matrix primarily controls the Weibull modulus ϱ. In the unaged samples $\varrho(= 4.4)$ is constant with x for $0 < x < 0.4$ and then at $x = 0.5\varrho$ decreases (to $\varrho = 2.8$) and approaches the value for pure PC. In the aged samples ϱ also appears to be

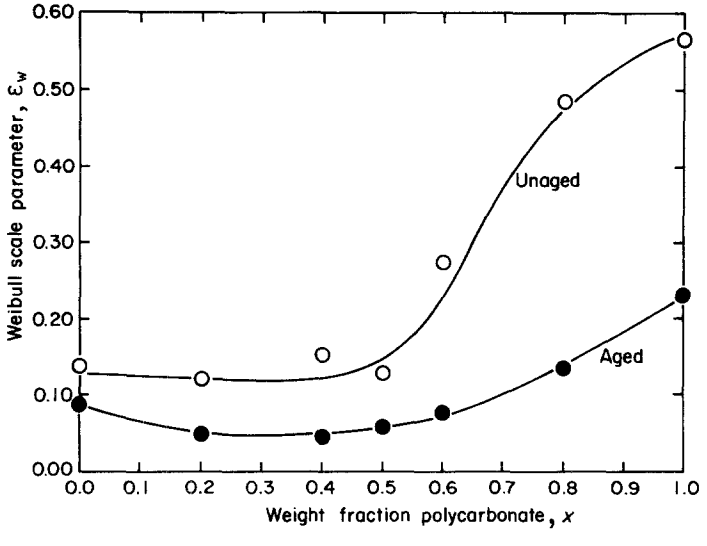

Figure 12 Weibull scale parameter ε_w as a function of x, weight fraction PC. (○) Unaged, (●) aged.

*The increase in drawing stress with strain has been corroborated in thin films ($\sim 2.0\,\mu$m thick) of pure PC using an Instron testing machine.

controlled by the deformation mechanism in the matrix.

Comparing Figs 4 and 12 shows that the Weibull scale parameter ε_w closely mirrors the median strain for void formation ε_v. Unlike ε_v, ε_w is a material constant and is independent of sample size [11]. Thus the Weibull analysis may be used to predict the median breakdown strains in macroscopic samples several orders of magnitude larger than our thin films.*

The slow strain rates employed in these experiments allow us to simplify the complicated process of void formation in phase separated systems. By examining the two pure polymers and each of the blends in the TEM, the mechanisms of the early stages of void formation in each phase may be determined at the submicrometre level. These experiments strongly suggest that dissimilar strain hardening rates for blends of glassy phases can control the breakdown mechanisms at the interface between the phases. To produce a high ε_v blend one requires a ductile matrix that strain hardens more rapidly than the inclusions. In addition we have also shown that by using a simple test the effects of physical ageing on void formation in thin films may be quantitatively determined.

5. Conclusions

1. PSAN and PC are only partially compatible and will phase separate.

2. Using a simple test quantitative information on the statistics of void and crack formation in thin films of homopolymers, copolymers and partially compatible blends may be determined.

3. In PSAN the median tensile strain for void formation ε_v was found to be ~ 0.13 whereas ε_v for PC exceeds 0.23.

4. In PSAN and PSAN-rich phases physical ageing suppresses shear deformation and predisposes the polymer to crazing. Because crazes are more susceptible to void formation than DZs physical ageing causes a decrease in ε_v. Similar ageing treatments in PC cause strain localization.

5. While the PSAN–PC interface does not fail by direct deadhesion craze breakdown to form voids in PSAN and PSAN-rich phases always occurs at the craze–bulk interface. Void formation in DZs (in PSAN and PC) occurs primarily by the debonding of the polymer from a dust particle at its initiation site.

6. The void formation statistics for partially compatible blends of PC and PSAN follow a Weibull distribution in strain.

7. Dissimilar strain hardening rates in glassy blends of phase separated polymers can control either craze or DZ breakdown to form voids. To produce a high ε_v blend requires a ductile matrix that strain hardens more rapidly than the inclusion.

Acknowledgements

We gladly acknowledge the financial support by the Cornell Materials Science Center for E. J. Kramer as well as the use of the facilities of the Cornell Materials Science Center which is funded by the NSF-DMR-MRL Program. L. L. Berger was partially supported by an IBM Polymer Science Fellowship. We also thank Professor S. L. Phoenix for many helpful discussions.

References

1. P. G. DEGENNES, "Scaling Concepts in Polymer Physics", (Cornell University Press, Ithaca, 1979) p. 103.
2. C. C. HSU and J. M. PRAUSNITZ, *Macromolecules* **7** (1974) 320.
3. I. C. SANCHEZ, *Polym. Eng. Sci.* **24** (1984) 79.
4. *Idem. Ann. Rev. Mater. Sci.* **13** (1983)
5. J. NOOLANDI, *Polym. Eng. Sci.* **24** (1984) 70.
6. J. S. HIGGINS and D. T. WALSH, *ibid.* **24** (1984) 555.
7. F. E. KARASZ and W. J. MACKNIGHT, "Structure and Prop. of Amorphous Polymers", edited by A. G. Walton (Elsevier, Amsterdam, 1978).
8. S. SAEKI, J. M. G. COWIE and J. J. MCEWEN, *Polymer* **24** (1983) 60.
9. A. BIRLEY and X. Y. CHEN, *British Polym. J.* **16** (1984) 77.
10. A. C. -M. YANG, E. J. KRAMER, C. C. KUO and S. L. PHOENIX, *Macromolecules,* **19** (1986) 2010.
11. *Idem, ibid.* **19** (1986) 2020.
12. B. D. LAUTERWASSER, PhD thesis, Cornell University (1979).
13. A. M. DONALD and E. J. KRAMER, *J. Mater. Sci.* **17** (1982) 1871.
14. *Idem, ibid.* **16** (1981) 2967.
15. N. VERHEULPEN-HEYMANS, *Polym. Eng. Sci.* **24** (1984) 809.
16. P. L. CORNES, I. C. SMITH and R. N. HAWARD, *J. Polym. Sci. Polym. Phys.* **15** (1977) 955.
17. K. SMITH and R. N. HAWARD, *ibid.* **18** (1977) 745.
18. N. WALKER, R. N. HAWARD and J. N. HAY, *J. Mater. Sci.* **14** (1977) 1085.
19. W. WEIBULL, *J. Appl. Mech.* **18** (1951) 293.
20. W. FELLER, "An Introduction to Probability Theory and its Applications", Vol. 3rd edn, (Wiley, New York, 1967) p. 147.
21. E. J. KRAMER, *Polym. Eng. Sci.* **24** (1984) 761.
22. C. S. HENKEE and E. J. KRAMER, *J. Polym. Sci. Polym. Phys.* **22** (1984) 721.
23. R. BRAGLIA and T. CASIRAGHI, *J. Mater. Sci.* **19** (1984) 2643.
24. T. T. WANG, M. MATSUO and T. K. KWEI, *J. Appl. Phys.* **42** (1971) 4188.
25. J. H. GOLDEN, B. L. HAMMANT and E. A. HAZELL, *J. Appl. Polym. Sci.* **11** (1967) 1571.
26. K. NEKI and P. H. GEIL, *J. Macromol. Sci.* **B2** (1968) 13.
27. G. A. ADAM, A. CROSS and R. N. HAWARD, *J. Mater. Sci.* **10** (1975) 1582.

Received 27 May
and accepted 18 August 1986

*The thin film nature of these experiments must be emphasized. In these samples only a small lateral constraint develops normal to the film surfaces (i.e. $\sigma_{zz} = 0$) whereas for macroscopic samples a non-zero σ_{zz} may change the deformation mechanism from shear (ductile) to crazing (brittle).